Polyethylene glycol phase change material embedded in a hierarchical porous carbon with superior thermal storage capacity and excellent stability

FENG Dai-Li[1,2*] ZANG Yu-Yang[1] LI Pei[1] FENG Yan-Hui[1, 2*] YAN Yu-YING[3] ZHANG Xin-Xin[1, 2]

(1. School of Energy and Environmental Engineering, University of Science and Technology Beijing, Beijing, 100083, China;

2. Beijing Key Laboratory of Energy Conservation and Emission Reduction for Metallurgical Industry, University of Science and Technology Beijing, Beijing 100083, China;

3. Fluids & Thermal Engineering Research Group, Faculty of Engineering, University of Nottingham, Nottingham NG7 2RD, UK

*Corresponding authors: dlfeng@ustb.edu.cn (Daili Feng); yhfeng@me.ustb.edu.cn (Yanhui Feng))

Abstract: Hierarchical porous materials are recommended to trade off the mismatch between high loading and efficient crystallization in pore-based composite phase change materials (PCMs), coupling the functions of expanded pores (mesopores and macropores) along with maintained micropores. Hierarchical porous carbon (HPC) was successfully synthesized from metal organic framework MOF-5 with a large specific surface area (1345 m^2/g) and high pore volume (2.69 cm^3/g). The adsorption capacity of HPC for low temperature phase change materials, polyethylene glycol (PEG) and stearic acid (SA) reaches over 90 wt%. The introduction of HPC has very little impact on the crystallinity of the PCMs, as a result, the composites possess similar high thermal storage capacity to pure PCM. The as-prepared composites efficiently perform heat store and release with reasonable reliability. Moreover, the supercooling of PCM was strongly suppressed due to the large surface area of HPC. Molecular dynamics (MD) simulation confirms that the smaller pores enable a stronger force of the carbon skeleton on the PCM, which ensures effective anchoring of the PCM. Simultaneously, those larger pores provide enough space for storage of PCM, with a reduced negative effect on its crystallization. After the compounding, the phonon vibration matching between guest and host is strengthened, which is beneficial to the transfer of energy thus receives an enhanced thermal conductivity. Our research demonstrates the great potential of using hierarchical porous skeleton to immobilize phase change materials for practical thermal storage.

Keywords: hierarchical porous carbon; polyethylene glycol; shape-stabilized phase change material; molecular dynamics simulation; thermal properties

1. Introduction

With the increasingly serious dual crisis of the energy and environment caused by the consumption of fossil fuels, there is a growing awareness of using new energy technologies, especially the most abundant solar radiation. However, a new energy has common shortcomings of intermittent and volatility in practical applications and is recommended to be converted into thermal energy and stored in energy storage materials [1]. As the main energy storage medium in latent heat storage, solid-liquid phase change materials (PCMs) realize high energy storage density and bridge the time gap between energy supply and demand via the process of phase change. Today, scientists and engineers continue to deal with leakage, corrosion of surroundings and low thermal conductivity remain in PCMs. Therefore, the idea of filling PCMs into porous materials is proposed for addressing the above issues. This kind of composite PCMs offers higher phase transition enthalpy and improved thermal conductivity under the premise of the good package, expanding the application range of the energy storage materials and becoming a cutting-edge topic in recent years [2-7].

The progress of the pore-derived shape-stabilized PCMs (ssPCMs) is mainly driven by the development of porous materials in recent decades. So, it is a step-by-step process from macropore towards nanopore, to achieve better immobilizing via a stronger capillary force [8]. Based on the reviewing of state-of-the-art researches, the nanoporous ssPCM is hard to realize the tradeoff between loading, crystallization, easy fabrication and package, limitations are hard to break through (Fig. 1). Generally speaking, the loading and crystallization ratio of PCM could barely exceed 70% for nanopore-based ssPCMs [8-10]. At present, there is a pressing need for porous materials that are able to support massive PCMs without any leakage.

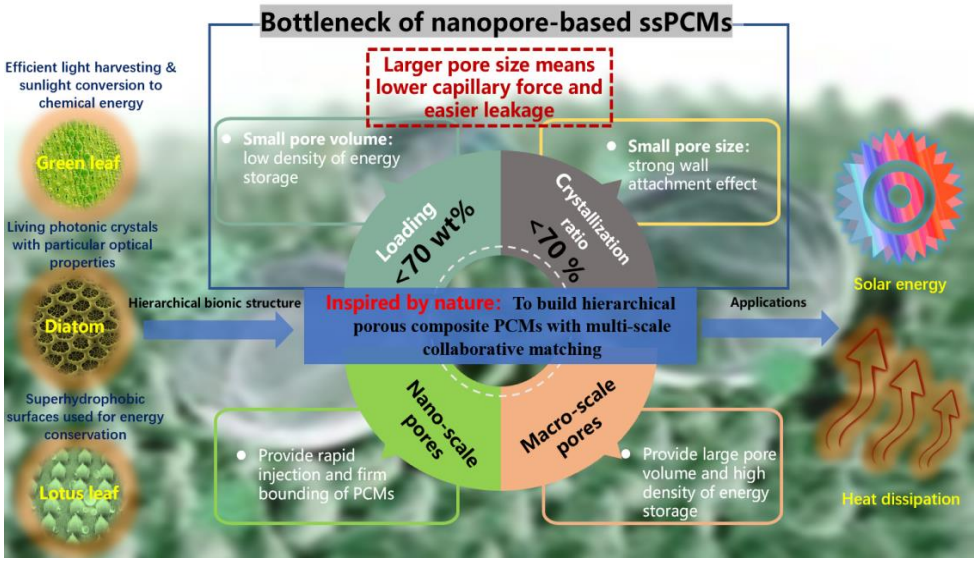

Fig. 1 Nanopore limitations and advantages of bio-inspired multiscale structures.

Dealing with the challenges and also inspired by nature, many biological materials derive their special functions through a multiscale organization of their structure, and hierarchy is one of the most typical features found everywhere in natural materials. The structural hierarchies contribute a lot to developing different functions, especially in energy-involved natural processes as the biological systems are maintained by the flow of energy (Fig. 1). The hierarchy of materials on pore size, pore arrangement, and pore shape which is desired to offer a combination of exceptional properties acting at different scales (nano-scale and macro-scale), would endow materials with ultra-high performance in thermal energy storage (Fig. 1). The hierarchical porous material possesses a controllable multistage pore structure, large specific surface area and extremely high pore volume. These characteristics make it superior to single-aperture porous materials in wide range functional adaptions such as adsorption [11], catalysis [12], thermal energy storage [13], hydrogen storage [14], coating [15], and sensing [16]: the developed multistage pore structure offers the material a large contact area, high capacity for storage and diffusion. Among all kinds of porous materials with graded structure, hierarchical porous carbon (HPC) has collected a wide range of attention with respect to strong skeleton rigidity, chemical stability, high thermal conductivity, and designable topology. At present, HPC with various structural forms has been obtained by different synthetic methods, including template method [17-19], template activation

phase combination method [20] high-temperature carbonization method, etc. [21-23]. It is worth mentioning that the metal-organic frameworks (MOFs) with a three-dimensional fully-through ordered pore structure [24-26] have emerged in recent years to provide a new template for the preparation of HPC.

HPC might be a real opportunity for preparing novel ssPCMs: the presence of large pores enables high storage capacity of the PCM with a limited negative effect on its crystallization thus guarantees a high energy storage density. Also, the capillary force induced by the microporous and mesoporous channels is able to perform firm anchoring of the PCM, further the thermal stability of the guest-host composite is maintained. However, up to now the reports regarding HPCs for latent heat thermal energy storage are scarce. Tang et.al. [13] first synthesized HPCs based composite PCMs, the PCM had been well encapsulated even under high loading. But the very little researches on HPC ssPCMs have paid attention to the preparation and thermal measurement with only one kind of PCM involved, and the knowledge of heat storage performance is still far from comprehensive understanding. Furthermore, the coupling effect attributed by macro-meso-micro multiscale collaboration on adsorption, crystallization and heat transfer behaviors of HPC-based ssPCMs has not been reported yet.

Herein, macro-meso-microporous structured HPC was firstly derived from metal-organic framework MOF-5. PEG with suitable phase transition temperature (46 ℃-65 ℃) and stable performance was selected as the phase change material, which has higher energy storage density (145 J/g-175 J/g) than other PCMs [27] at the similar phase change temperature. Meanwhile, another PCM, stearic acid (SA), a commonly used fatty acid, which has a phase transition temperature of 30-70 ℃ and a high melting latent heat of 140-250 J/g, was also filled into HPC to confirm the universal reliability of the skeleton. Existing studies have shown that the composite PCMs using PEG and SA as core materials exhibit good thermal properties and therefore have a wide range of applications in the thermal energy storage fields such as thermal management of electronics [28], building insulation [29] and light–heat conversion [30]. The combination of core material and HPC was realized through the melt impregnation method. A systematic investigation of structural and thermal properties was delivered after then.

The large specific surface area and the large pore volume of HPC supplied sufficient space to store PCMs and are responsible for the much-reduced supercooling degree. The obtained ssPCMs exhibited high thermal storage capacity, efficient energy absorbing-releasing, good thermal stability and enhanced thermal conductivity. The molecular dynamics (MD) simulation was performed to gain insight into the functions of the HPC structure at different levels of hierarchy. From the explanation for experimental phenomena via a molecular level analysis, we are trying to look into the mechanism on high adsorption capacity and excellent heat storage behavior of the HPC-derived composites. This work is aiming to provide a basic understanding of energy storage and transfer in a multi-scale material and offer suggestions for the future design of hierarchical porous composite PCMs.

2. Experimental

2.1 Synthesis

The purity and commercial company information on the employed materials were shown in **Table S1**. The synthesized procedure of MOF-5 material is referenced from the literature [31]. Then, the MOF-5 powder was placed in an alumina boat, heated to 1000 ℃ at a rate of 5 ℃/min and maintained for 6 h under N_2 atmosphere in a tube furnace, and then cooled to room temperature. The PEG@HPCs were prepared by physical impregnation at standard atmospheric pressure. The weight of PEG and HPC was determined according to the formula of PEG mass fractions (mass fraction $\omega = \frac{W_{PEG}}{W_{PEG}+W_{HPC}}$). The first step was to dissolve the PEG in absolute ethanol (The reason for choosing this particular solvent was shown in the **Supporting Information**), and then the HPC was added under magnetic stirring at 80 ℃ for 3 h to fuse the mixture completely. Finally, the mixed solution was dried at 80 ℃ (higher than the PEG melting temperature) until complete removal of the ethanol. The PEG@HPC composites with different PEG mass fractions can be obtained by changing the initial weight of PEG and HPC. SA@HPCs were prepared following the same procedure. The final composite sample on a white filter was heated at an over-melting temperature for 2 h to observe whether oil stains appeared on the filter paper, thus to determine PCM

leaked out or not (leakage test).

2.2 Characterization

The X-ray diffraction (XRD, Smartlab3) was used to test the phase composition of the samples. The test range is 10-90° (2θ), with a scanning rate of 10°/min. The microstructures of HPCs were investigated by scanning electron microscopy (SEM, ZEISS SUPRA55) and transmission electron microscopy (TEM, JEM-2100F). Thermal gravimetric analysis (TGA, SDT Q600) was conducted to analyze the weight loss during carbonization with a 10 ℃/min heating rate of under N_2 atmosphere. Argon adsorption-desorption was applied on a surface area and porosity analyzer (Micromeritics ASAP 2460) to determine the pore volume and surface area at 87 K. The Density functional theory (DFT) model was used to predict the pore size distribution. The phase change temperature and the enthalpy of the samples were tested by differential scanning calorimetry (DSC, TA SDT-Q600) with a heating rate of 10 °C/min, and the flow rate of constant nitrogen stream is 100 ml/min. All samples in the tests mentioned above are powder. The thermal conductivity was derived from specific heat capacity, thermal diffusivity and the density obtained by laser flash (LFA, NETZSCH LAF467 HyperFlash) measurement, which needs the powder sample to be compressed into a 6.4 mm radius tablet with a pressure of 5 tons and a thickness of 2-3 mm.

3. Simulation methodology

3.1 Force field

In MD simulations, the Tersoff [32] potential was used to describe the C–C interactions within the HPC, and the CVFF force field was employed for interactions between atoms of the PEG molecules. The LJ potential was assigned to compute non-bonding interactions between HPC and PEG, and the LJ parameters were derived according to the Lorenz-Bethelot mix rule. The parameters were all listed in **Table S2**.

3.2 Mean square displacement (MSD) method for melting point calculation

The melting temperature of PEG bulk and PEG@HPC composites was simulated via the MSD method, which was discussed in detail (**Supporting Information)**.

4. Results and discussion

4.1 Characterization

4.1.1 Structure characterization of HPC

The HPC was derived from carbonization of MOF-5. TGA results show that the MOF-5 carbonization has gone through three stages of weight loss (Fig. 2a): the evaporation of solvent molecules in the pores below 300 ℃, the decomposition of the MOF-5 skeleton and the conversion of Zn^{2+} to ZnO, and the evaporation of CO_2, CO and ZnO at 500~1000 ℃.

To understand the change of phase composition after carbonization, the samples of MOF-5 and HPC was investigated by XRD. As shown in Fig.2b, the experimental and reported XRD patterns trend to agree confirms that the prepared sample had the crystal structure of MOF-5 [33]. However, the characteristic peaks of ZnO disappear and there is no sharp peak after carbonization (Fig.2c), indicating that ZnO evaporated and the derived HPC was amorphous. Dispersed and weak XRD peaks locate at around ~24° and ~43°, corresponding to carbon (002) and (101) diffraction, identify the disordered micro-graphitized structure of HPC.

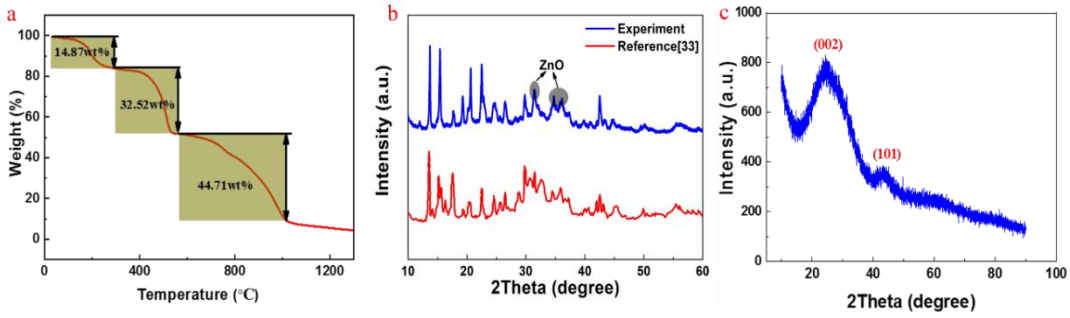

Fig. 2 (a) TGA diagram of MOF-5 carbonization process, XRD pattern of (b) MOF-5[33] (c) HPC.

The hierarchy in HPC structure is produced following the procedure of nucleation, migration, aggregation and evaporation of ZnO particles [13]. During the carbonization, the MOF-5 skeleton decomposes and small ZnO particles appear. As time increases, small ZnO particles begin to migrate and aggregate into larger clusters. Massive micro-scaled and meso-scaled channels were produced by the migration of ZnO clusters, meanwhile, the nano-scaled cavities were generated by the evaporation of ZnO clusters. The presence of ~10 nm mesopores and ~1 μm macropores can be clearly observed in

the TEM (Fig. 3Aa) and SEM (Fig. 3Ab) images.

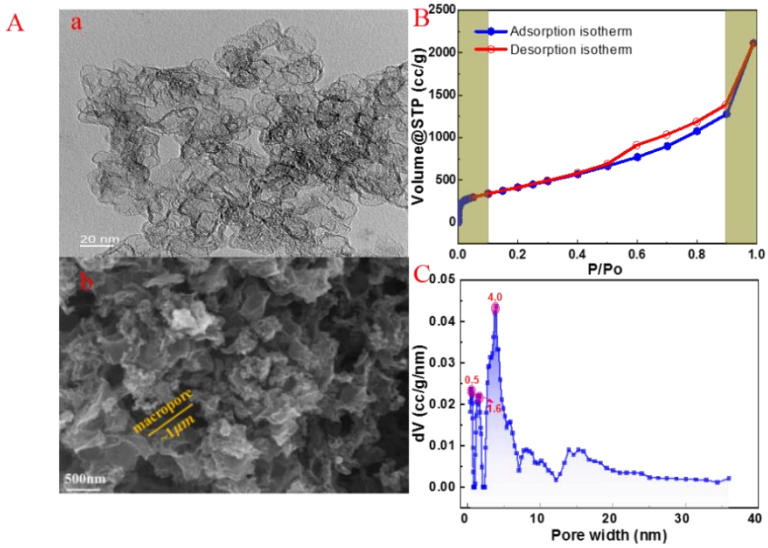

Fig. 3 (A) Images of HPC (a) TEM, (b) SEM, (B) argon adsorption-desorption isotherm, (C) pore size distribution.

The argon sorption isotherms were applied to further illustrate the porous structure of the HPC. The adsorption-desorption results of HPC (Fig. 3B) display typical type IV isotherms, indicating the presence of micropores, mesopores and macropores. The BET specific surface area is 1345 m^2/g, which is lower than the reference value [13], and the total pore volume is 2.688 cm^3/g, which is comparable to the literature [13]. Analyzing by DFT method, the pore diameters are mainly 0.5 nm and 1.6 nm for micropores, and 4.0 nm for mesoporous (Fig. 3C). These collected parameters are references for building molecular models.

4.1.2 Structure characterization of PEG@HPCs

The SEM microscopy (Fig. 4A) and leakage test (Fig. 4B) of PEG@HPC composites with different PEG mass fractions were applied to studied the shape stabilizing performance and determine the maximum loading of HPC to PEG. As shown in Fig. 4Ad, excessive PEG was attached on the surface of HPC until the loading of PEG was reached up to 95 wt%, and the oil stain (Fig.4B) also suggests an overload of PEG at 95 wt%. So, the maximum load of PEG in HPC is confirmed to be 92.5 wt%. After 50 times of heating-cooling repeats, no leakage of liquid PEG was observed in 92.5 wt% PEG@HPCs, indicating that it has good thermal stability. At the maximum loading, the PEG has substantially occupied all the pores of HPC (Table 1). For packing

SA, the maximum storage could reach up to 90 wt% as well (Table 1).

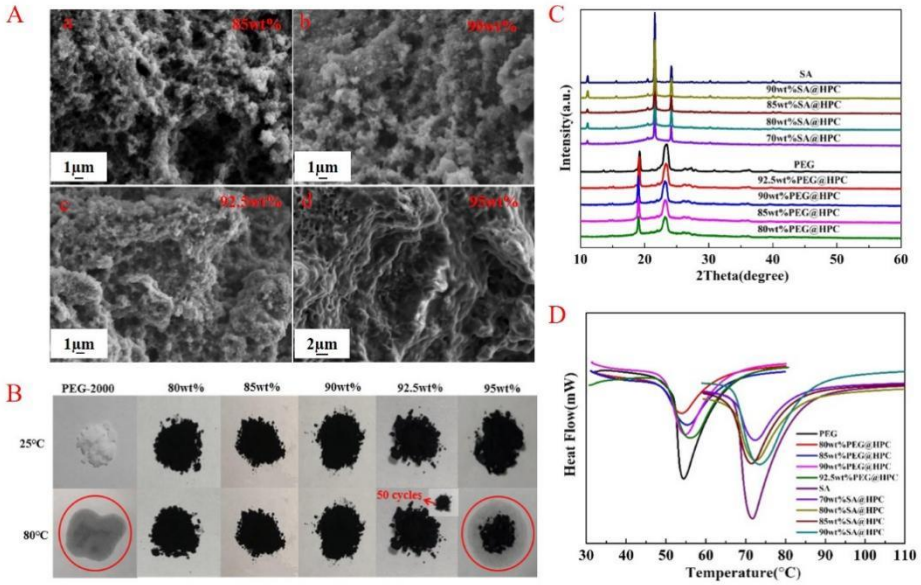

Fig. 4 (A) SEM images of composite phase change material with different PEG mass fractions (a) 85 wt% (b) 90 wt% (c) 92.5 wt% (d) 95 wt%, (B) Leakage test diagram of composite phase change materials with different PEG mass fractions, (C) XRD patterns of PEG, SA and their composites, (D) heat flow curves versus temperature of PEG, SA and their composites

Table 1 Argon adsorption-desorption measurements of surface area and pore volume

Sample	BET surface area, m^2/g	Pore volume, cm^3/g
HPC	1345	2.688
80 wt% PEG@HPC	18.22	0.047
85 wt% PEG@HPC	12.02	0.026
90 wt% PEG@HPC	7.44	0.007
92.5 wt% PEG@HPC	4.28	0.007
70 wt% SA@HPC	49.82	0.155
80 wt% SA@HPC	28.29	0.086
85 wt% SA@HPC	0.72	0.026
90 wt% SA@HPC	7.91	0.015

XRD patterns of PEG@HPC composites were tested to investigate the influence of HPC on PEG crystallization. As shown in Fig. 4C, the two diffraction peaks at 18.9° 23.3° denoted the crystal structure of PEG-2000. They are maintained in PEG@HPC without generating new peaks, claiming that the crystallization process of PEG would not be affected by the introduction of HPC, and there is only a physical combination of the guest and the host. Besides, the intensity of peaks was enhanced with the increased weight percentage of PEG. Meanwhile, the crystal structure of SA was also maintained in HPC even at 90 wt% loading (Fig. 4C). Thus, HPC is a kind of ideal skeleton that enables large storage of PCM with a completely preserved crystal structure and phase change function.

4.2 Thermal properties of HPC derived ssPCMs

The phase change temperature and latent heat of HPC-based ssPCMs were measured by DSC as shown in Fig. 4D and Table 2, 3. Specifically, the theoretical enthalpy of the composites was calculated as follows:

$$\Delta H_{m,theory}(\Delta H_{f,theory}) = wt\% \times \Delta H_{m,PCM}(\Delta H_{f,PCM}) \quad (1)$$

where $\Delta H_{m,theory}$ and $\Delta H_{f,theory}$ corresponds to the theoretical melting and freezing enthalpy of the composites, respectively. $wt\%$ stands for the mass percentage of the PCM in the composites, and $\Delta H_{m,PCM}$ and $\Delta H_{f,PCM}$ refers to the tested melting and cooling enthalpy of the pure PCM, respectively.

Followed, we analyzed the thermal characteristics of phase change composites in detail from the aspects of supercooling, heat storage efficiency, thermal stability and thermal conductivity.

Table 2 Thermal properties of PEG@HPC composites

Sample	T_m/T_f, ℃	$\Delta H_m/\Delta H_f$, J·g^{-1}	$\Delta H_{m,theory}/\Delta H_{f,theory}$, J·g^{-1}
PEG-2000	52.48/19.18	153.0/151.5	-
80wt%PEG@HPC	48.36/25.27	64.5/61.7	122.4/121.2
85wt%PEG@HPC	49.16/29.83	88.2/79.9	130.1/128.7
90wt%PEG@HPC	49.74/35.84	118.5/113.0	137.7/136.3
92.5wt%PEG@HPC	50.01/35.51	128.2/123.2	141.5/140.1
50 cycles	50.96/35.20	126.4/119.8	141.5/140.1

Table 3 Thermal properties of SA@HPC composites

Sample	T_m, ℃	ΔH_m, J·g^{-1}	$\Delta H_{m,theory}$, J·g^{-1}
SA	67.73	204.0	-
70wt%SA@HPC	67.08	92.0	142.8
80wt%SA@HPC	66.86	116.4	163.2
85wt%SA@HPC	66.00	145.5	173.4
90wt%SA@HPC	67.01	158.6	183.6

4.2.1 Supercooling suppression

Supercooling (T_m-T_f) is ubiquitous during phase transition and served as a primary condition for triggering crystallization. However, the large extent of supercooling is a problematic existence that leads to the decrease of crystallization temperature and the delay of crystallization of PCMs, so that the latent heat stored cannot be released in time. The temperature mismatch between storage and exothermic heat reduces the utilization efficiency of thermal energy, thus greatly limits the PCMs'

further application. After compounding, the melting point of the material is slightly reduced (Table 2, 3), which is caused by the scale effect [34]. Interestingly, the difference between melting temperature and cooling temperature of PEG was significantly reduced under the influence of HPC. As shown in Fig. 5a, the supercooling degree of free PEG is 33.3 ℃, then gradually narrowing with an increased mass fraction of PEG in the composite, and finally decreases to 14 ℃, with a suppression ratio nearly 60%. The cause of this phenomenon is that the HPC can provide numerous sites for heterogeneous nucleation of PEG, benefits from the large interfacial surface area [35] offered by HPC. Interestingly, the supercooling degree was further alleviated by 5 ℃ compared with the single scale mesoporous carbon loaded PEG [36], identifying the superiority of hierarchy in the structure. The suppression of supercooling results in an accelerated crystallization process of the novel ssPCMs which builds up the potential for real application.

4.2.2 Heat storage capacity and efficiency

Generally speaking, the introduction of the porous skeleton has a negative effect on the crystallinity of PCM and results in a reduced heat storage capacity [37,38]. Here, the crystallization efficiency θ was used to reflect the impact of HPC on the crystallization of the PCM confined in the pores:

$$\theta = \frac{\Delta H_{\mathrm{m,comp}}(\Delta H_{\mathrm{f,comp}})}{\Delta H_{\mathrm{m,theory}}(\Delta H_{\mathrm{f,theory}})} \times 100\% \quad (2)$$

Where $\Delta H_{\mathrm{m,comp}}$ and $\Delta \mathrm{H}_{\mathrm{f,comp}}$ represents to the melting and solidification latent heat of ssPCMs obtained by the DSC test, respectively. The theoretical enthalpy is calculated by the Eqs. (1). The crystallization efficiencies derived from melting enthalpies and cooling enthalpies (Fig. 5b) are presented in Fig. 5c. Furthermore, the encapsulation fraction F (Fig. 5c) and heat storage efficiency E (Fig. 5d) were evaluated by Eqs. (3) and (4):

$$F = \frac{\Delta H_{\mathrm{m,comp}}}{\Delta H_{\mathrm{m,PCM}}} \times 100\% \quad (3)$$

$$E = \frac{\Delta H_{\mathrm{m,comp}} + \Delta H_{\mathrm{f,comp}}}{wt\% \times (\Delta H_{\mathrm{m,PCM}} + \Delta H_{\mathrm{f,PCM}})} \times 100\% \quad (4)$$

As depicted, the mass fraction of PEG in the composite increases, the enthalpy gradually increases (Fig. 5b), very close to that of pure PEG. As shown in Fig. 5c, for

92.5 wt% PEG@HPCs, 90.6% of the confined PEG crystallizes with an encapsulation fraction of 83.8%, and the corresponding heat storage capacity is up to 128.2 J/g. Due to the high adsorption capacity of HPC, more PCMs were stored in the pores thus strengthened the intermolecular interaction within the PCM and weakened the interaction with HPC, thereby leading to high crystallinity. What is more, the thermal energy could be efficiently stored and released in a melting-freezing cycle with a heat storage efficiency of 89.3% (Fig. 5d). These results confirmed that although a fraction of PCM still failed to crystallize, the HPC minimized this negative function of interfacial effect on crystallization attributed to the presence of macropores, thus guaranteed the high heat storage performance. SA@HPCs also possess ideal thermal properties with a heat storage capacity of 158.6 J/g and a crystallization efficiency of 86.4% (Fig. 5c). Those results of PEG@HPC and SA@HPC suggested that almost all the PCM encapsulated in HPC could effectively perform solid to liquid phase transition with efficient thermal energy storage and vice versa.

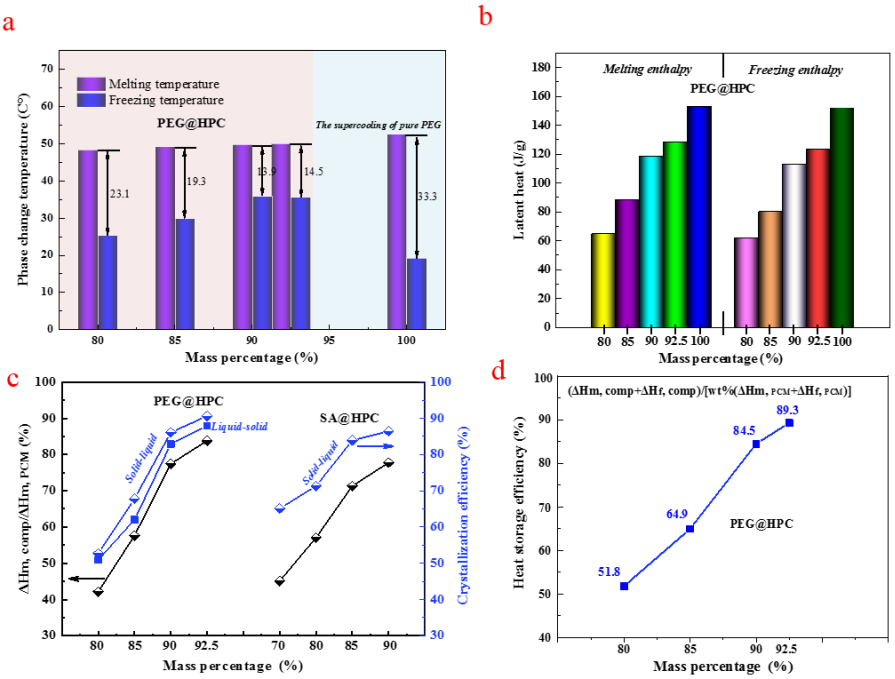

Fig. 5 Heat storage performance of (a) supercooling of PEG in composites (b) enthalpies during heating and cooling of PEG@HPC (c) encapsulation fraction and crystallization efficiency of PEG@HPC and SA@HPC (d) heat storage efficiency of PEG@HPC

As the most commonly used PCMs, PEG and SA have been packed with many nanoporous materials, and their corresponding storage performances were displayed in Fig. 6, and compared with those of HPC composites. HPC shows obvious advantages over other

counterparts attributed to its hierarchy in pore structure, in line with our expectations. Specially, wrapping the PCMs in the capsule to construct core/shell structure can also make the composite materials have a high latent heat. The latent heat of the composite using organosilica shells to encapsulate docosane is as high as 143 J/g [39]. It is worth noting that the latent enthalpy of the SA@HPC composite material in this work is comparable to that of the docosane@organosilica material.

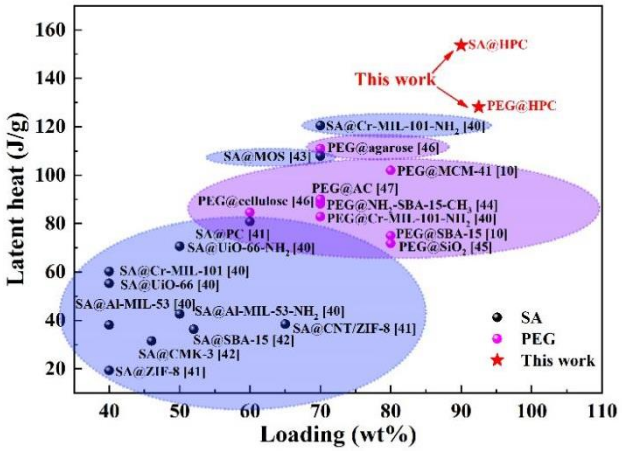

Fig. 6 The thermal energy storage capacity of PEG and SA in HPC compared with other nanoporous skeletons[10,40-47]

4.2.3 Thermal stability

During the thermal energy storage process, the maintenance of phase change properties is critical to the application of a novel ssPCM. The thermal stability of 92.5 wt% PEG@HPC was evaluated after 50 melting-cooling repeated cycles. The phase change temperature, melting/freezing enthalpy, and the shape have negligible changes (Table 2, Fig. 4B). Likewise, the advantages of supercooling degree and heat storage efficiency were all preserved. It indicated the composite ssPCM has high reliability in thermal energy storage.

4.2.4 Thermal conductivity

The low thermal conductivity is one of the persistent bottlenecks for efficient energy harvesting using ssPCMs. Improvement in thermal conductivity of ssPCM is of particular importance for the rapid charging and discharging of thermal energy. The thermal conductivity of the novel ssPCM was measured via the laser flashing (LFA) method. The thermal diffusivity and specific heat at temperature T were obtained

directly by the LFA. Then, the thermal conductivity of the sample could be derived according to Equation 5:

$$\lambda(T) = \alpha(T) \times C_p(T) \times \rho(T) \quad (5)$$

where λ is the thermal conductivity of the sample, W/(m·K); α is the thermal diffusivity, mm^2/s; ρ is the sample density, g/cm^3; C_p is the specific heat capacity, J/(g·K).

The thickness of the PEG sample was 2.2 mm, and the mass was weighted to be 302 mg. The 92.5 wt% PEG@HPC sample tablet was 2 mm thick with a weight of 300 mg. Then, the volume v and density ρ of the sample were obtained according to Equation 6 and 7. All the parameters were listed in Table 4, and the corresponding thermal conductivity of PEG was 0.274 W/(m·K), which was comparable to the measured value reported in the literature [13]. The thermal conductivity of 92.5 wt% PEG@HPC was 0.312 W/(m·K), which was higher than that of PEG, indicating that the existence of a lightweight porous carbon skeleton has a positive contribution to the overall thermal conductivity of the composite.

$$v = \pi r^2 h \quad (6)$$

$$\rho = \frac{m}{v} \quad (7)$$

Table 4. LFA measurement

Sample	Thermal diffusivity mm^2/s	Specific heat J/(g·K)	Density g/cm^3	Thermal conductivity W/(m·K)
PEG	0.144	1.720	1.107	0.274
92.5 wt% PEG@HPC	0.164	1.629	1.166	0.312

Compared with similar nanoporous composite materials (Fig.7), the heat transfer capability of PEG@HPC composite is better than that of the metal organic framework (SA@ZIF-8) and ordered mesoporous silica (PEG@MCM-41), and about the same with carbon based (SA@PC) composites. However, the thermal conductivity of the SA@Cr-MIL-101-NH_2 material is higher than that of PEG@HPC composite, because the amino function of Cr-MIL-101 constructs hydrogen bonds thus provides a heat transfer pathway. This offers a strategy to further improve the thermal conductivity of HPC derived composite phase change material.

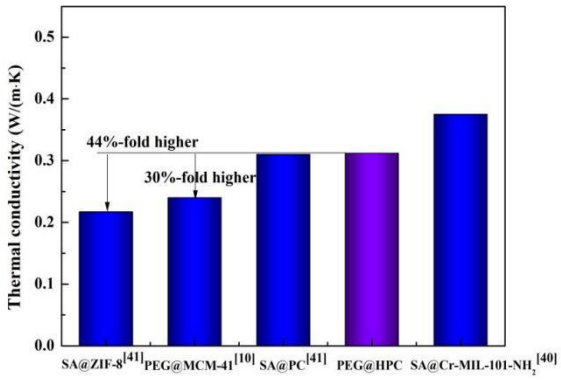

Fig.7 Comparison of thermal conductivity with other nanoporous skeletons[10,40,41]

4.3 Mechanism of phase change thermal characteristics

Here, we delivered a comprehensive theoretically analysis on the phase change and energy transfer mechanism via MD simulation The contribution of pores at different scales to thermal energy storage and their coupling effect on heat transfer was emphasized.

4.3.1 Model construction and validation

The model construction of microporous amorphous carbon, HPC, PEG and the verification of HPC model were shown in the **Supporting Information**. We finally obtained the HPC model with a diameter of 1.6 nm along the X and Y axes and a diameter of 4 nm along the Z axis. The combination of PEG-2000 with HPC as a composite is shown in Fig. 8.

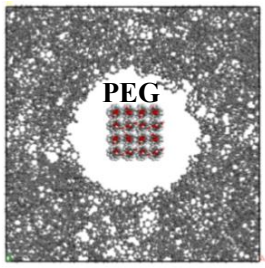

Fig. 8 The composite of PEG@HPC

4.3.2 Pore size effect

In the HPC structure, the adsorption of PEG molecular chains may be greatly affected by the pore size. With this regard, the adsorption process of PEG into HPC was simulated. PEG molecular chains were placed on the topside of the 4 nm channel to be adsorbed naturally (Fig. 9). The PEG molecular chains first agglomerate and then enter the 4 nm pore. The adsorption state is stable at a simulation time of 3000 ps. When the PEG molecular chains are completely introduced, some of the PEG molecular chains are further

adsorbed into the 1.6 nm pores and firmly bound. The overall process could be visualized in **Supporting video S1 and S2**. However, when the molecular chains were started from the topside of 1.6 nm channel, only a few PEG molecular chains were adsorbed in but failed to go further into the 4 nm mesopores. So, the smaller pore has a stronger driving force to suck PEG from the large pore to the small one than vice versa, and the stronger suction will also perform the better confining ability. On the other hand, PEG, as a polymer, prefers to enter large pores first and then move into small pores to get firmly immobilized to prevent leakage. That is the idea of hierarchical pores that we want to make.

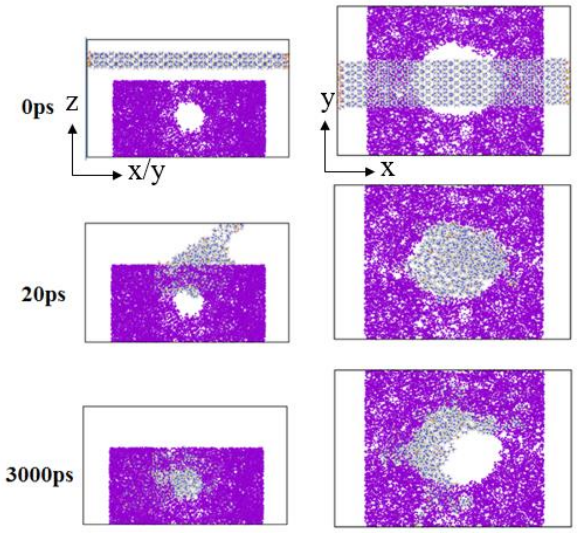

Fig. 9 The adsorption process of PEG molecular chain

To further analyze the influence of different pore sizes on the guest-host interaction, amorphous carbon models with pore diameters of 1.6 nm (21.36 Å ×21.36 Å ×128.18 Å) and 4 nm (64.09 Å ×64.09 Å ×128.18 Å) are established separately and then filled with the same amount of PEG molecular chains.

The interaction energy between the PCM material and the skeleton was calculated [48] and it is larger in the 1.6 nm porous carbon (Fig. 10). The results coincide with the adsorption behavior that provides a piece of evidence for a stronger interaction in small pores.

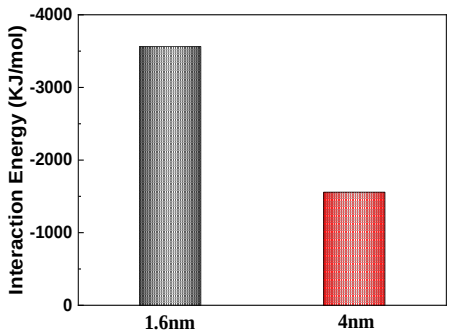

Fig.10 Interaction energy between PEG and HPC

Furthermore, the interaction force between HPC and PEG is specified by the atom-atom radial distribution function $g(r)$ [49]. The selected atom pairs are most likely to form hydrogen bonding: the oxygen and hydrogen atoms at the end of the PEG molecular chains, the carbon atoms in the inner wall of the skeleton, as shown in Fig. 11. For the 1.6 nm system, the value of the first peak is higher with a corresponding position much closer to 2 Å (hydrogen bonding distance), compared with that of the 4 nm system (Fig. 12). It indicates that the smaller the pore size, the stronger the interaction force within the atom pairs, thus the stronger the force that carbon skeleton applied to the PEG molecular chains. It is beneficial to achieve the high stability of the composite PCMs. The weak interaction force attributed by large pores reduces the wall attachment effect of PEG chains, and PEG is much easier to crystallize, according to our previous works [37,38]. As for the PEG in those macropores, they are almost impermeable to interfacial effects and can crystallize completely. This is the critical advantage benefits from the multistage porous structure, successfully integrates the massive loading, high crystallinity and effective packaging.

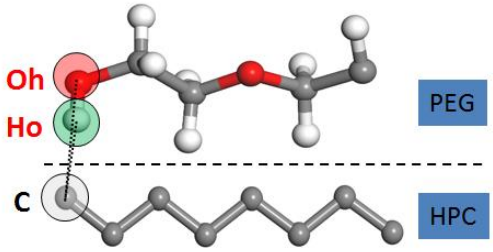

Fig. 11 The motifs of atomic pairs

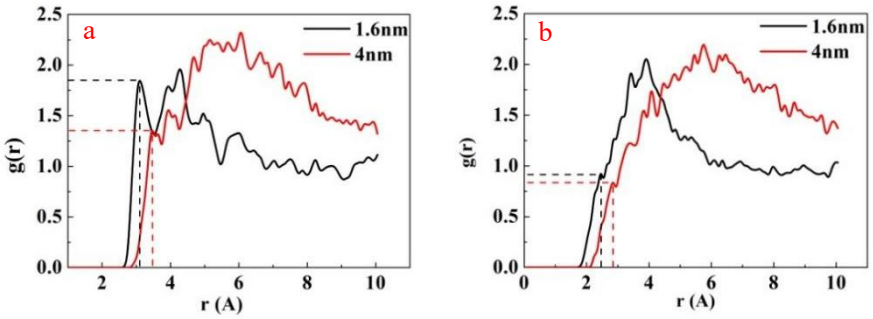

Fig. 12 Radial distribution function diagram (a) Oh-C (b) Ho-C

4.3.3 Analysis of phase transition characteristics

The self-diffusion coefficients of PEG bulk and composites are shown in Fig. 13a, and it is linear with the temperature. But there is an inflection point, indicating that the self-diffusion ability of the material changes before and after the phase change, which is regarded as the melting point,

The melting temperature of the PEG@HPC is 324.5 K, a little bit lower than that of the bulk PEG (343.0 K), which is consistent with the experimental results. Besides, the error of the melting point between MD and DSC is within 5%. So, the models and simulation methods are profitable for predicting PEG@HPC.

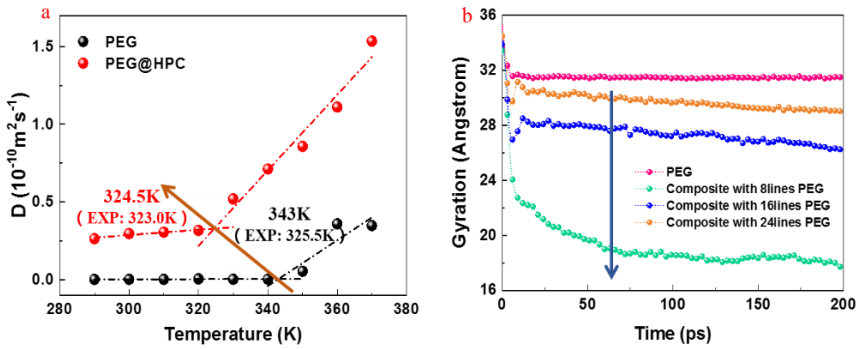

Fig. 13 (a) Self-diffusion coefficient as a function of temperature, (b) the radius of gyration before and after compounding

Using the radius of gyration to reflex the flexibility of the PEG segment [50], further the mechanism of the difference in the phase change point of PEG is explored. The radius of gyration of the PEG after filling is reduced (Fig. 13b), indicating that the PEG molecular segment is more flexible in the nanoconfined space due to the guest-host interaction, resulting in a reduced melting temperature. As the number of the PEG chains increases, the radius of gyration increases and approaches to that of the PEG block. More chains will strengthen the interaction within PEG to preserve the initial molecular structure. So, the melting point of composite material increases with the

growing PEG loading, which shows a good match with the experimental trend.

4.3.4 Heat conduction analysis

The thermal conductivity of PEG@HPC is measured to be higher than pure PEG. Here, the local heat flux is computed to directly observe the difference in heat transfer caused by the filling of PEG. Both ends of the model were fixed, the energy generated by the motion of every atom and the interaction energy between atoms were summed to obtain the heat flux. A slice in the middle of the models with 6 Å thickness was selected as the computational domain, and the time step was 0.1 fs with a total simulation time of 700 ps. The first 200 ps was applied for reaching an equilibrium state, and the followed 500 ps was used to collect data for the local heat flux.

The local heat flux of each atom in the calculated slice was normalized and then projected on the x-y plane (Fig. 14). High heat flow was colored in red. In the PEG@HPCs, the number of atoms with high heat flux (red spots) is slightly higher than that of HPC, indicating that the local heat flow is increased, and the filling of PEG contributes to the minor improvement of the thermal conductivity of the composite system.

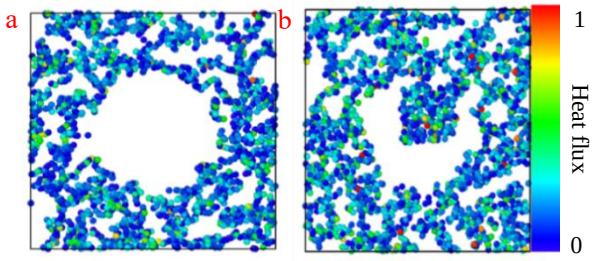

Fig. 14 Projection of local heat flow in the x-y plane (a) HPC (b) PEG@HPC

The vibration of the atom near the equilibrium point is the intrinsic cause of energy transfer [51]. Calculating the vibration density of states (VDOS), the difference of thermal conductivity of the system before and after the combination is explored. For the PEG (Fig. 15a), the vibration is mainly in the range of 30-50 THz and 80-100 THz. While after compounding, the high-frequency phonon vibration is enhanced, and the overall vibration frequency is shifted to the left. For the substrate HPC (Fig. 15b), it is mainly in the range of 0-20 THz. The low-frequency phonon vibration is weakened, and the vibration peak appears in the intermediate frequency region in the composites (Fig. 15c), indicating that PEG excites the mid-frequency phonon vibration of HPC, which is beneficial to the phonon vibration matching between PEG and HPC thus enhances energy transfer.

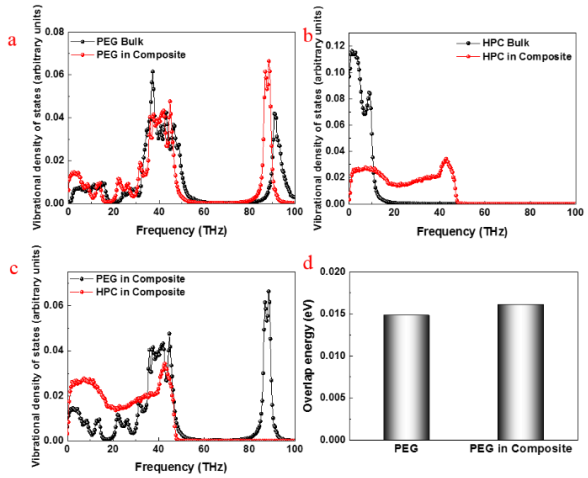

Fig. 15 VDOS before and after combination (a) PEG (b) HPC, (c) VDOS of PEG@HPC, and (d) Overlap phonon energy of C-O in PEG

In order to analyze the heat transfer process between atoms, the overlap phonon energy is calculated to further quantify the vibration density of states [52]. For PEG, since the repeat unit is C-C-O, so the C-O bond is the weak link of heat transfer, which is critical to heat transfer. The overlap phonon energy of the C-O bond in PEG before and after compounding is calculated (Fig. 15d). After recombination, it increases between C-O atoms, and the phonon vibration matching is enhanced. It is beneficial to energy transfer and the enhancement of thermal conductivity, consistent with the calculation result of VDOS.

5. Conclusions

The melt impregnation method was used to prepare phase change composites of HPC filled with PEG and SA. The structure and thermal properties were comprehensively characterized, and the contribution of pores at different scales to thermal energy storage and their coupling effect on heat transfer were analyzed by MD. The main conclusions are as follows：

(1) HPC prepared by high-temperature carbonization of MOF-5 has a high surface area (1345 m^2/g) and a large total volume (2.69 cm^3/g). The structure characters are responsible for the strong suppression of supercooling in phase transition. The HPC demonstrates the excellent capacity in loading and immobilizing with an almost negligible effect on the crystallization of both PEG and SA. The maximum loading and crystallization efficiency of PEG and SA are more than 90%, and the heat

storage capacity is comparative to pure PCM.

(2) The MD simulation predicts that the radius of gyration of the PEG is reduced after filling, indicating that the PEG chain has better flexibility in the confined space, thus there is a decrease in the melting point. The simulated adsorption process identifies that PEG chains are preferred to be adsorbed into big pores first before entering small pores and could be firmly immobilized. The interaction energy and the radial distribution function show that the smaller the pore size of HPC, the stronger the guest-host force on the PEG. So, the hierarchy in pore structure is confirmed to be beneficial to massive loading and crystal structure maintaining as well as shape stabilizing of PCMs.

(3) The thermal conductivity of PEG@HPC is 0.312 W/m·K, which is higher than that of the PEG. According to the results of vibrational dynamic density and overlapping energy, the phonon vibration matching after compounding is improved further contributes to heat transfer.

This presented work confirms the idea of using a hierarchical structure to break through the limitations of ssPCMs based on the single-scale nanoporous skeleton, and receives high thermal energy storage performance as expected. This work can serve as a suggestion for the future design of hierarchical porous composite PCMs to meet the coupling of functions at different scales. For example, build the graded channels/pores from present random distribution into an ordered, progressive structure, going towards ultimate thermal-targeted energy storage ssPCMs.

Acknowledgments

This work is financially supported by the National Key R&D Program of China (No. 2018YFA0702300), National Natural Science Foundation of China (No. 51876007), Beijing Natural Science Foundation (No.3192022) and Fundamental Research Funds for the Central Universities (FRF-BD-20-09A).

References

[1] Wang Y, Xia D, Feng H. Research Progress of Organic Phase Change Thermal Storage Materials[J]. Materials Review A: Review, 2011, 25(2): 66-74.

[2] Wu S, Li T, Tong Z, et al. High-performance thermally conductive phase change

composites by large-size oriented graphite sheets for scalable thermal energy harvesting[J]. Advanced Materials, 2019, 31(49):1905099.

[3] Wu S, Li T, Wu M, et al. Highly thermally conductive and flexible phase change composites enabled by polymer/graphite nanoplatelet-based dual networks for efficient thermal management[J]. Journal of Materials Chemistry A, 2020, 8(38): 20011-20020.

[4] Li T, Lee J H, Wang R, et al. Enhancement of heat transfer for thermal energy storage application using stearic acid nanocomposite with multi-walled carbon nanotubes[J]. Energy, 2013, 55:752-761.

[5] Li T X , Lee J H , Wang R, et al. Heat transfer characteristics of phase change nanocomposite materials for thermal energy storage application[J]. International Journal of Heat and Mass Transfer, 2014, 75:1–11.

[6] Wu S , Li T, Yan T, et al. High performance form-stable expanded graphite/stearic acid composite phase change material for modular thermal energy storage[J]. International Journal of Heat and Mass Transfer, 2016, 102:733-744.

[7] Wu D, Wen W, Chen S, et al. Preparation and Properties of a Novel Form-Stable Phase Change Material Based on a Gelator[J]. Journal of Materials Chemistry A, 2015, 3(6): 2589-2600.

[8] Feng D, Feng Y, Qiu L, et al. Review on nanoporous composite phase change materials: Fabrication, characterization, enhancement and molecular simulation. Renewable and Sustainable Energy Reviews,2019,109:578-605.

[9] Han L, Ma G, Xie S, et al. Preparation and characterization of the shape-stabilized phase change material based on sebacic acid and mesoporous MCM-41. Journal of Thermal Analysis and Calorimetry 2017, 130 (2), 935-941.

[10] Feng L, Zhao W, Zheng J, et al. The shape-stabilized phase change materials composed of polyethylene glycol and various mesoporous matrices (AC, SBA-15 and MCM-41). Solar Energy Materials and Solar Cells 2011, 95 (12), 3550-3556.

[11] Hu Y, Tong X, Zhuo H, et al. 3D hierarchical porous N-doped carbon aerogel from renewable cellulose: an attractive carbon for high-performance supercapacitor electrode and CO2 adsorption[J]. Rsc Advances, 2016, 6(19):15788-15795.

[12] Shen K, Zhang L, Chen X, et al. Ordered macro-microporous metal-organic framework single crystals[J]. Science, 2018, 359(6372):206-210.

[13] Tang J, Yang M, Dong W, et al. Highly porous carbons derived from MOFs for shape-stabilized phase change materials with high storage capacity and thermal conductivity[J]. Rsc Advances, 2016, 6(46):40106-40114.

[14] Hu X, Chen Q, Zhao Y, et al. Facile synthesis of hierarchical triazine-based porous carbons for hydrogen storage[J]. Microporous&Mesoporous Materials, 2016, 224:129-134.

[15] Li Y, Zhang Z, Ge B, et al. One-pot, template-free synthesis of robust

superhydrophobic polymer monolith with adjustable hierarchical porous structure[J]. Green Chemistry, 2016, 18(19): 5266-527.
[16] Zhu G, Xu H, Xiao Y, et al. Facile Fabrication and Enhanced Sensing Properties of Hierarchically Porous CuO Architectures[J]. Acs Applied Materials & Interfaces, 2012, 4(2):744-751.
[17] Strubel P, Thieme S, Biemelt T, et al. ZnO Hard Templating for Synthesis of Hierarchical Porous Carbons with Tailored Porosity and High Performance in Lithium-Sulfur Battery[J]. Advanced Functional Materials, 2015, 25(2):287-297.
[18] Wang S, Chen S, Wei Q, et al. Bioinspired Synthesis of Hierarchical Porous Graphitic Carbon Spheres with Outstanding High-Rate Performance in Lithium-Ion Batteries[J]. Chemistry of Materials, 2015, 27(1):336-342.
[19] Liu Y, Lin B, Li D, et al. Magnetically-separable hierarchically porous carbon monoliths with partially graphitized structures as excellent adsorbents for dyes[J]. Journal of Porous Materials, 2014, 21(6):933-938.
[20] Liu W, Xu B, Liu L. Hierarchical porous carbon prepared by NaOH activation of nano-CaCO 3 templated carbon for high rate supercapacitors[J]. New Journal of Chemistry, 2014, 38(11):5509-5514.
[21] Jeon J W, Sharma R, Meduri P, et al. In situ one-step synthesis of hierarchical nitrogen-doped porous carbon for high-performance supercapacitors[J]. Acs Applied Materials & Interfaces, 2014, 6(10):7214-7222.
[22] Li X. Preparation of Structure Controllable Carbon Materials by Block Copolymer Charring Method and Electrochemical Properties[D]. Lanzhou University of Technology, 2013.
[23] Silvestre-Albero A, Silvestre-Albero J, Martínez-Escandell M, et al. Micro/mesoporous activated carbons derived from polyaniline: promising candidates for CO2 adsorption[J]. Industrial & Engineering Chemistry Research, 2014, 53(40): 15398-15405.
[24] Silva P, Vilela S M, Tomé J P, et al. Multifunctional metal-organic frameworks: from academia to industrial applications[J]. Chemical Society Reviews, 2015, 44(19):6774-6803.
[25] Eddaoudi M, Sava D F, Eubank J F, et al. Zeolite-like metal–organic frameworks (ZMOFs): design, synthesis, and properties[J]. Chemical Society Reviews, 2015, 44(1): 228-249.
[26] Furukawa H, Cordova K E, O'Keeffe M, et al. The chemistry and applications of metal-organic frameworks[J]. Science, 2013, 44(45):1230444.
[27] Sharma A , Tyagi V V , Chen C R , et al. Review on thermal energy storage with phase change materials and applications[J]. Renewable and Sustainable Energy Reviews, 2009, 13(2):318-345.
[28] Jiang Y, Wang Z, Shang M, et al. Heat collection and supply of interconnected

netlike graphene/polyethyleneglycol composites for thermoelectric devices[J]. Nanoscale, 2015,7:10950–10953.
[29] Tatsidjodoung P, Pierres N L, Luo L. A review of potential materials for thermal energy storage in building applications[J]. Renewable and Sustainable Energy Reviews, 2013, 18:327-349.
[30] Li B, Nie S, Hao Y, et al., Stearic-acid/carbon-nanotube composites with tailored shape-stabilized phase transitions and ligth-heat conversion for thermal energy storage[J]. Energy Conversion and Management, 2015,98: 314-321.
[31] Hu J, Wang H, Gao Q, et al. Porous carbons prepared by using metal–organic framework as the precursor for supercapacitors[J]. Carbon, 2010, 48(12):3599-3606.
[32] Lindsay L, Broido D. Optimized Tersoff and Brenner empirical potential parameters for lattice dynamics and phonon thermal transport in carbon nanotubes and graphene [J]. Physical Review B, 2010, 81(20): 205441.
[33] Srinivas G, Krungleviciute V, Guo Z X, et al. Exceptional CO2 capture in a hierarchically porous carbon with simultaneous high surface area and pore volume[J]. Energy & Environmental Science, 2014, 7(1): 335-342.
[34] Antoniammal P, Arivuoli D. Size and shape dependence on melting temperature of gallium nitride nanoparticles[J]. Journal of Nanomaterials, 2012, 2012(5):3517-3526.
[35] Kholmanov I, Kim J, Ou Eric, Ruoff R S, Shi L. Continuous Carbon Nanotube–Ultrathin Graphite Hybrid Foams for Increased Thermal Conductivity and Suppressed Subcooling in Composite Phase Change Materials[J]. ACS Nano, 2015, 9(12): 11699-11707.
[36] D Feng, P Li, Y Feng, et al. Using mesoporous carbon to pack polyethylene glycol as a shape-stabilized phase change material with excellent energy storage capacity and thermal conductivity[J]. Microporous and Mesoporous Materials, 2021, 310:110631.
[37] Feng D, Feng Y, Li P, Zang Y, Wang C, Zhang X. Modified mesoporous silica filled with PEG as a shape-stabilized phase change materials for improved thermal energy storage performance. Microporous Mesoporous Mater 2020; 292:109756.
[38] Feng D, Feng Y, Zang Y, Li P, Zhang X. Phase change in modified metal organic frameworks MIL-101 (Cr): mechanism on highly improved energy storage performance. Microporous Mesoporous Mater 2019; 280:124–32.
[39] Fredi Giulia, Dirè Sandra, Callone Emanuela, et al. Docosane-Organosilica Microcapsules for Structural Composites with Thermal Energy Storage/Release Capability.[J]. Materials, 2019,12:1286.
[40] Luan Y, Yang M, Ma Q, et al. Introduction of an organic acid phase changing material into metal–organic frameworks and the study of its thermal properties[J].

Journal of Materials Chemistry A, 2016, 4(20): 7641-7649.
[41] Li A, Wang J, Dong C, et al. Core-sheath structural carbon materials for integrated enhancement of thermal conductivity and capacity[J]. Applied Energy, 2018, 217:369-376.
[42] Kadoono T, Ogura M. Heat storage properties of organic phase-change materials confined in the nanospace of mesoporous SBA-15 and CMK-3[J]. Physical Chemistry Chemical Physics, 2014, 16(12):5495-5498.
[43] Gao J, Lv M, Lu J, et al. Enhanced thermal properties of novel latent heat thermal storage material through confinement of stearic acid in meso-structured onion-like silica[J]. JOM, 2017, 69(12): 2785-2790.
[44] Wang J, Yang M, Lu Y, et al. Surface functionalization engineering driven crystallization behavior of polyethylene glycol confined in mesoporous silica for shape-stabilized phase change materials[J]. Nano Energy, 2016, 19:78-87.
[45] Yang H, Feng L, Wang C, et al. Confinement effect of SiO2 framework on phase change of PEG in shape-stabilized PEG/SiO2 composites[J]. European Polymer Journal, 2012, 48(4):803-810.
[46] Sentürk S B, Kahraman D, Alkan C, et al. Biodegradable PEG/cellulose, PEG/agarose and PEG/chitosan blends as shape stabilized phase change materials for latent heat energy storage[J]. Carbohydrate Polymers, 2011, 84(1):141-144.
[47] Wang C, Feng L, Li W, et al. Shape-stabilized phase change materials based on polyethylene glycol/porous carbon composite: the influence of the pore structure of the carbon materials[J]. Solar Energy Materials and Solar Cells, 2012, 105: 21-26.
[48] Yang M J, Stipp S L S, Harding J. Biological control on calcite crystallizationby polysaccharides, Cryst. Growth Des. 11(2008) 4066–4074.
[49] Kun Wang, Ya-fan Zhao, Gui-wu Lu, Yu-liang Wang, Ju-na Chena, De-zhi Su. Molecular dynamics study on conguration energy and radial distribution functions of ammonium dihydrogen phosphates solution[J]. Chin. J. Chem. Phys., 2014(27):380-386.
[50] Wanga Y, Wang W, Zhang Z, Xu L, Li P. Study of the glass transition temperature and the mechanical properties of PET/modified silica nanocomposite by molecular dynamics simulation[J]. European Polymer Journal 2016 (75) :36–45.
[51] Loong C K, Vashishta P, Kalia R K, et al. Phonon density of states and oxygen-isotope effect in Ba1-xKxBiO 3. Physical Review B, 1992, 45(14): 8052.
[52] Zhang X, Jiang J. Thermal Conductivity of Zeolitic Imidazolate Framework-8: A Molecular Simulation Study[J]. The Journal of Physical Chemistry C, 2013, 117(36):18441-18447.